

In situ confinement of ultra-small Pd clusters within nanosized silicalite-1 zeolite for high-efficient hydrogen generation catalysis

Ning Wang,^{†‡} Qiming Sun,^{†‡} Risheng Bai,[†] Xu Li,[†] Guanqi Guo,[†] Jihong Yu^{†*}

[†]State Key Laboratory of Inorganic Synthesis and Preparative Chemistry, College of Chemistry, Jilin University, Changchun 130012, P. R. China

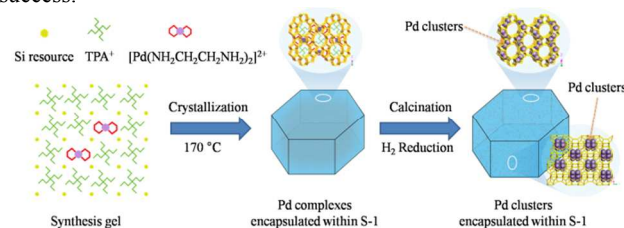
ABSTRACT: Well-dispersed and ultra-small Pd clusters in nanosized silicalite-1 (MFI) zeolite have been firstly prepared under direct hydrothermal conditions using $[\text{Pd}(\text{NH}_2\text{CH}_2\text{CH}_2\text{NH}_2)_2]\text{Cl}_2$ as precursor. High resolution STEM studies indicate that the Pd clusters are encapsulated within the intersectional channels of MFI and the Pd clusters in adjacent channels visually aggregate forming nanoparticles of *ca.* 1.8 nm. The resultant catalysts show an excellent activity and highly efficient H_2 generation toward the complete decomposition of formic acid (FA) under mild conditions. Notably, thanks to the further reduced Pd nanoparticle size (*ca.* 1.5 nm) and the additionally introduced basic sites, the Pd/S-1-in-K catalyst afforded turnover frequency (TOF) values up to 856 h^{-1} at 25°C and 3027 h^{-1} at 50°C , respectively. The easy-to-fabricate in situ confinement synthesis of metal clusters in zeolites endows the catalysts with superior catalytic activities, excellent recyclability and high thermal stability, thus opening new perspectives for the practical application of FA as a viable and effective H_2 storage material for fuel cells.

Hydrogen (H_2) is considered to be an environmentally attractive fuel and a promising efficient energy carrier for future applications because of its high energy density and renewability.¹ However, safe and efficient storage and release of H_2 remains a bottleneck and challenge for the fuel cell based hydrogen economy.² Recently, formic acid (FA), as a product of biomass possessing a high H_2 content (4.4 wt%), non-toxicity, easy recharging, and outstanding stability has proven to be a safe and suitable hydrogen carrier for portable hydrogen storage application.³ Hydrogen stored in FA can be released via a dehydrogenation pathway ($\text{HCOOH} \rightarrow \text{H}_2 + \text{CO}_2$) over suitable catalysts. However, in view of the perspective of hydrogen storage application, the undesired dehydration reaction ($\text{HCOOH} \rightarrow \text{H}_2\text{O} + \text{CO}$) should be avoided because CO is easy to make the catalyst poisoning in fuel cells.⁴

In recent years, lots of homogeneous catalysts have been intensively investigated showing excellent performance for the FA dehydrogenation.⁵ However, several drawbacks such as fast deactivation, difficult to separate and recycle, and using organic solvents hinder their further utility in applications. To overcome these shortcomings, heterogeneous catalysts have attracted tremendous and increasing interest.^{3c, 6} Several types of support materials of metal nanoparticles (NPs) have been employed in FA decomposition reactions, such as graphene oxide,⁷ nanoporous carbon,^{3d} MOFs,^{4a, 8} etc. However, some of these catalysts suffer

from the relatively poor recyclability and lower thermal stability. Hence, developing highly efficient and stable catalysts for FA decomposition remains a challenge.

Zeolites have drawn growing attention as the ideal supports for confinement synthesis of the metal NPs due to their well-defined channels, tunable acidity and basicity, highly thermal and chemical stability.⁹ The zeolite matrix could restrain the aggregation of the metal NPs, thus enhance the catalytic activity and recycling stabilities of the catalysts. In general, the NPs were supported onto zeolites by ion-change¹⁰ and wetness impregnation.¹¹ However, these methods may lead to large and non-uniform NPs as well as poor dispersion and unsatisfied catalytic activity.¹² Recently, Iglesia and co-workers developed the synthetic protocols for encapsulating series of smaller metal clusters within different types of aluminosilicate zeolites such as BEA, FAU, SOD, LTA, etc. by ligand-stabilized method and MFI via interzeolite transformation.¹³ Notably, silicalite-1 with MFI zeotype is an ideal catalyst support for numbers of industrial processes. However, up to now, in situ encapsulating ultra-small metal clusters within MFI structure under direct hydrothermal conditions remains no success.



Scheme 1. Schematic of the process for confinement synthesis of Pd clusters within nanosized S-1 zeolite.

Herein, ultra-small Pd clusters encapsulated within nanosized silicalite-1 (S-1) zeolite have been for the first time successfully synthesized under direct hydrothermal conditions using $[\text{Pd}(\text{NH}_2\text{CH}_2\text{CH}_2\text{NH}_2)_2]\text{Cl}_2$ as precursor and tetrapropylammonium hydroxide (TPAOH) as template. The resultant catalysts exhibit superior activity and efficient H_2 generation without CO toward the complete decomposition of FA. Strikingly, when the KOH was introduced into the synthesis gel, the Pd/S-1-in-K catalyst with basic sites and further reduced size of metal clusters show enhanced catalytic activity affording excellent TOF values as high as 856 h^{-1} at 25°C and 3027 h^{-1} at 50°C , respectively, which is among the highest activity for heterogeneously catalyzed FA decomposition under similar conditions.

Ultra-small Pd clusters in-situ encapsulated within nanosized S-1 zeolite (Pd/S-1-in) were synthesized in a starting gel with the

molar composition of 1.0SiO₂: 0.4TPAOH: 35H₂O: 0.0045[Pd(NH₂CH₂CH₂NH₂)₂]Cl₂ under hydrothermal conditions at 170 °C for 4 days followed by H₂ reduction. The Raman spectroscopy, TG-DTA, and ¹³C MAS NMR analyses confirm that the [Pd(NH₂CH₂CH₂NH₂)₂]Cl₂ complex keeps intact inside the as-synthesized zeolite (Figures S1~S3). To generate basicity in the Pd/S-1 catalysts that may benefit the cleavage of the O-H bonds in FA molecules and further improve the activity of FA decomposition,^{7a} NaOH and KOH were for the first time introduced into the synthesis gel to prepare Pd/S-1-in-Na and Pd/S-1-in-K, respectively, under the similar condition to Pd/S-1-in. The synthetic process of Pd/S-1-in catalyst is illustrated in Scheme 1. Firstly, the Pd complexes interact with the initial zeolitic gel and are encapsulated into the zeolite framework by self-assembly during crystallization process. Upon calcination in air and reduction by H₂, the ultra-small Pd clusters can be finally confined inside the nanosized silicalite-1 zeolite. The specific sites of Pd clusters within the S-1 zeolite will be discussed in the later section. For comparison, the Pd/S-1-im catalyst was also synthesized by impregnation using incipient wetness method with (NH₄)₂PdCl₄ solution; the Pd/C catalyst was obtained from commercial Pd/C catalyst followed by H₂ reduction treatment at 200 °C for 2 h.

As shown in Figure S4, the XRD patterns of all of the Pd clusters-containing zeolite catalysts show characteristic diffraction peaks of the **MFI** structure, without detectable peaks corresponding to Pd or oxide crystal structures, indicating the absence of large Pd species in the as-synthesized samples.

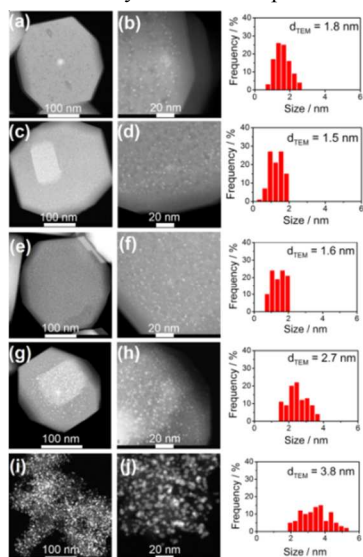


Figure 1. STEM images of Pd/S-1-in (a, b), Pd/S-1-in-K (c, d), Pd/S-1-in-Na (e, f), Pd/S-1-im (g, h), and Pd/C (i, j) samples and corresponding size distributions of Pd clusters. Surface weighted mean cluster diameter $d_{\text{TEM}} = \sum n_i d_i^3 / \sum n_i d_i^2$, where n_i is the number of crystallites having diameter d_i .

Transmission Electron Microscope (TEM) images and scanning transmission electron microscope (STEM) images as well as the Pd clusters size distributions of the synthesized samples after calcination and H₂ reduction are shown in Figure S5 and Figure 1. TEM images show that the Pd clusters encapsulated within nanosized S-1 zeolites are well dispersed and uniformly distributed throughout the zeolite crystals. The average sizes of Pd clusters in situ encapsulated within the nanosized S-1 zeolite are in the range of 1.5~1.8 nm, which are much smaller than those of impregnation-prepared Pd/S-1-im catalyst (2.7 nm) and the commercial Pd/C catalyst (3.8 nm). Notably, the introduction of alkali hydroxide in the synthesis gel could further decrease the Pd clusters size

because the alkali cations may reduce some void spaces of the channels.

It should be noticed that the visually observed sizes of Pd nanoparticles appear much larger than those of **MFI** channels (0.53 × 0.56 nm) as well as intersectional channels (~0.9 nm).¹⁴ High resolution STEM was used to investigate the location of Pd clusters inside the crystals of sample Pd/S-1-K. The intact and empty straight channels can clearly be observed (Figure 2a), indicating that most of the Pd clusters might be located in the intersectional void spaces between the straight and sinusoidal channels of the **MFI** structure. When the view is changed to another orientation, the Pd clusters turn into the rod-like aggregates encapsulated inside the channels (Figure 2b). Corresponding schematic crystallographic projections of Pd clusters in S-1 are also shown in Figure 2c and 2d. Strikingly, the ultra-small Pd clusters (0.3~0.6 nm) in the Pd/S-1-in catalyst can be observed (Figure S6). The large size of Pd nanoparticles observed in Figure 1 might be due to the visual aggregation of Pd clusters within the adjacent channels. In addition, all of the calcined zeolitic samples show almost the same ²⁹Si MAS NMR spectra (Figure S7), which further demonstrates that the encapsulated Pd clusters did not break the zeolite framework and the zeolite framework keeps intact.

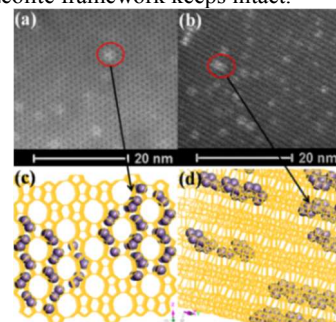


Figure 2. High resolution STEM images (a, b) of Pd/S-1-K sample and corresponding schematic crystallographic projections (c, d) of **MFI** with different orientations.

Simulated annealing calculations were also performed using UFF force field to study the location of the guest species in the channels. Figure S8 presents the optimal structure model with the lowest energy. The results show that the tetrapropylammonium cations (TPA⁺) locate in the centre of the straight 10-ring channels along the *b* direction and the [Pd(NH₂CH₂CH₂NH₂)₂]²⁺ cations in the intersectional channels. Some hydroxyl anions also exist in the structure of crystals for balancing the positive charges. After removing the TPA⁺ and ethylenediamine ligands, the simulation results indicate that the ultra-small Pd clusters are preferably located in the intersectional void spaces between the straight and sinusoidal channels, which is in accordance with the observed STEM images.

To further identify that the Pd clusters are encapsulated within the zeolite crystals rather than on the crystal surface, the shape-selective reduction of nitrobenzene and 3-nitrotoluene were performed over the Pd/S-1-in catalyst as compared with the Pd/C catalyst. According to the UV/vis spectra and GC-MS analyses (Figures S9~S13), the Pd/C catalyst exhibited the 100% conversion for the reduction of both nitrobenzene and 3-nitrotoluene. In contrast, the Pd/S-1-in catalyst only showed the 100% conversion for the reduction of nitrobenzene, but no activity for the reduction of 3-nitrotoluene that cannot enter into the zeolite channels due to its bulky molecule size. These results further prove that the Pd clusters are encapsulated inside the zeolite crystals instead of located on the crystal surface.

The STEM image of Pd/S-1-in-K, corresponding HAADF-STEM images and elemental mappings for Si, Pd, and K elements

are shown in Figure S14. It can be seen that the Pd and K elements are uniformly distributed throughout the S-1 zeolite crystals. The energy-dispersive X-ray (EDX) spectrum further confirms the existence of Pd and K in the sample. All of the Pd clusters-containing zeolites possess the similar metal loading amount of approximately 0.63–0.65 wt% by inductively coupled plasma atomic emission spectroscopy (ICP-AES) analysis (Table S1) and the amounts of Na and K are 0.21 wt% and 0.62 wt% in samples Pd/S-1-in-Na and Pd/S-1-in-K, respectively. N₂ adsorption measurements show that some decrease of micropore area of *ca.* 20 m²/g can be observed for Pd/S-1-in samples as compared to the S-1 zeolite, indicating that the dispersed Pd clusters are occupied inside the pores of S-1 zeolites. However, the Pd/S-1-in sample still possesses sufficient void space (191 m²/g) for the reactant transfer (Figure S15). CO₂-TPD profiles reveal that the Pd/S-1-in-Na and Pd/S-1-in-K samples possess some basicity due to the introduction of alkali cations onto the zeolite (Figure S16).¹⁵ Moreover, the Pd clusters dispersion values estimated from H₂ chemisorption of sample Pd/S-1-K are maximum compared to other samples, indicating that more metal cluster surfaces are available for catalytic reaction (Table S1).

The X-ray photoelectron spectroscopy (XPS) spectrum of the Pd/C sample (Figure S14c) shows two peaks at 335.7 eV and 341.0 eV that are attributed to the Pd3d_{5/2} and Pd3d_{3/2} of Pd(0), respectively.^{3d} However, no XPS signals can be observed in Pd/S-1-K because the Pd clusters were confined inside the zeolites. When the Pd/S-1-K sample was dissolved in NaOH solution, the peaks at 335.1 eV and 340.4 eV can be observed that correspond to the typical Pd metal with the valence of zero.¹⁶

Significantly, the sample Pd/S-1-in exhibited remarkably improved thermal stability compared to the Pd/C and Pd/S-1-im samples. As shown in Figure S17, after calcination at 700 °C for 2 h under N₂ atmosphere, the Pd particles in Pd/C almost entirely sintered, and the diameter of Pd particles increased from *ca.* 3.8 nm to *ca.* 27 nm. In contrast, the Pd/S-1-in sample showed less change of Pd particles size from *ca.* 1.8 nm to 2.3 nm. Moreover, the Pd/S-1-in sample also exhibited good stability in H₂ and O₂ atmosphere as well as by ageing treatments at 600 °C in the presence of water (Figures S18–20). After calcination, the morphology and crystallinity of Pd clusters-containing zeolites were still well kept (Figures S21–S24).

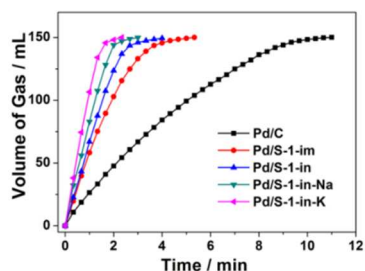


Figure 3. Volume of the generated gas (CO₂ + H₂) versus time for the dehydrogenation of FA-SF (1:1) solution over Pd/C and Pd/S-1 catalysts at 50 °C ($n_{\text{Pd}}/n_{\text{FA}} = 0.01$).

Catalytic activities for H₂ generation from the dehydrogenation of FA-sodium formate (SF) (1:1) at 25 °C and 50 °C are shown in Figure S25 and Figure 3, respectively. Compared to the Pd/C catalyst, Pd clusters-containing zeolite catalysts exhibited the complete decomposition of FA as well as superior activities. Moreover, the hydrogen production rates over the Pd/S-1-in catalysts synthesized by in situ encapsulated Pd clusters within nanosized S-1 zeolite are much faster than that over the impregnation-prepared catalyst Pd/S-1-im. Notably, the Pd/S-1-in-K catalyst generated 148 mL of gas without detectable CO (<10 ppm)

within 2.0 min ($n_{\text{Pd}}/n_{\text{FA}} = 0.01$, FA/SF = 1:1), which is important for fuel cell application, and the composition of generated gases has been confirmed by gas chromatography (GC) analyses (Figures S26 and S27). Moreover, the Pd/S-1-in-K catalyst gave the highest turnover frequency (TOF) of 856 h⁻¹ at 25 °C and 3027 h⁻¹ at 50 °C, respectively, which is of about 6-fold improvement compared to the Pd/C catalyst. These TOF values are among the highest activity for heterogeneously catalyzed FA decomposition under similar conditions^{3a, c, d, 4a} and even higher than most of the active homogenous catalysts (Table S2).^{5c, 17}

The superior catalytic activities for H₂ generation over Pd/S-1-in-K catalyst could be attributed to the ultra-small size of Pd clusters as well as the basicity generated by the introduction of alkali cations onto the zeolites that can act as a proton scavenger favorable for the cleavage of O-H bonds in the FA molecules and H₂ generation subsequently.^{7a} The rate of H₂ generation was determined to be 696 L H₂ h⁻¹ g_{Pd}⁻¹, which corresponds to a theoretical power density of 940 W h⁻¹ g_{Pd}⁻¹ for energy generation.^{3c} Assuming 60% operation efficiency and a typical energy requirement value of 0.5–2.0 W h for portable terminals, 0.14–0.56 g of the present Pd/S-1-in-K catalyst would be sufficient to supply H₂ for small proton exchange membrane fuel cell (PEMFC) devices.^{3d}

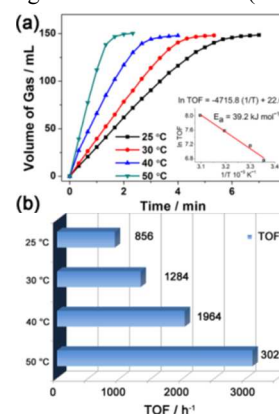


Figure 4. a) Volume of the generated gas (CO₂ + H₂) versus time and (b) corresponding TOF values of H₂ generation for the dehydrogenation of FA-SF (1:1) solution at different temperatures over Pd/S-1-in-K catalyst. Inset of (a): Arrhenius plot (ln TOF vs. 1/T).

Catalytic activities for H₂ generation from the dehydrogenation of FA-sodium formate (SF) (1:1) at 50 °C were also investigated over the Pd/S-1-in catalysts with different Pd loading contents. The catalysts with Pd loading contents of 0.47 wt% and 1.08 wt%, with visually observed nanoparticle sizes of 1.6 nm and 2.2 nm (Figure S28), give the turnover frequency (TOF) values of 2204 and 2119 h⁻¹, respectively, which are comparable with the TOF value of 2197 h⁻¹ of the above studied catalyst with Pd loading content of 0.64 wt% (Figure S29). This result further implies that the intrinsic metal cluster sizes of Pd inside the zeolite channels for catalysts with different Pd loading contents are in fact similar.

To investigate the effect of SF in the dehydrogenation of FA, different ratios of FA and SF were modulated for the Pd/S-1-in-K catalyst. As shown in Figure S30, the activities of FA decomposition improved with the increase of the molar percentage of SF in the SA-SF solution until the ratio of FA and SF reached to 1:1. After that further increasing the SF percentage had no effect on the FA decomposition. In addition, the reaction temperature also greatly affected the H₂ generation rates. With the increase of reaction temperature, the H₂ evolution rates were further enhanced (Figure 4 and Figure S31). The apparent activation energies (*E_a*) of Pd/S-1-in-K and Pd/S-1-in catalysts were 39.2 KJ mol⁻¹ and 42.8 KJ mol⁻¹, which are lower than most of those reported in

previous works for FA decomposition (Table S3), indicating that highly efficient H₂ generation from FA can be easily obtained at convenient temperature.¹⁸

The recycling stability of FA dehydrogenation over Pd/S-1-in-K and Pd/S-1-in catalysts was investigated. After completion of the previous run, the catalysts were recollected and dried for next recycle without reduction again. As shown in Figures S32 and S33, almost the same activities as the fresh catalyst were obtained over 5 cycles. In addition, after the catalytic reaction, the size distributions of Pd clusters as well as the morphology and crystallinity of the zeolite catalysts remained unchanged, suggesting that the catalysts of ultra-small Pd clusters encapsulated within nanosized silicalite-1 zeolites possessed superior recycling stabilities during FA decomposition (Figures S34–S38).

In summary, a facile strategy has been successfully developed to synthesize ultra-small Pd clusters encapsulated within the intersectional channels of nanosized silicalite-1 zeolite using [Pd(NH₂CH₂CH₂NH₂)₂]Cl₂ as precursor under direct hydrothermal conditions. The as-prepared catalysts show an excellent activity and highly efficient H₂ generation without CO toward the complete decomposition of FA in a FA-SF system under mild condition. Notably, the Pd/S-1-in-K catalyst with incorporated basicity affords the highest TOF values reaching up to 856 h⁻¹ at 25 °C and 3027 h⁻¹ at 50 °C, respectively, due to the further reduced Pd clusters size and introduced basic sites in zeolites. In addition, the as-synthesized catalysts possess superior thermal stabilities as well as excellent recycling stabilities during FA decomposition due to the good confinement of Pd clusters within the zeolite matrix. This work demonstrates that zeolites with well-confined nanospaces and shape-selectivity for molecules can be used as the excellent catalytic supports for well-dispersed and ultra-small metallic clusters. The superior catalytic activities, excellent recyclability, high thermal stability and easy-to-fabricate method of ultra-small metal clusters confined in zeolites create a new perspective for the practical application of FA as a viable and effective H₂ storage material for fuel cells.

ASSOCIATED CONTENT

Supporting Information

This material is available free of charge via the Internet at <http://pubs.acs.org>.

AUTHOR INFORMATION

Corresponding Author

*E-mail: jihong@jlu.edu.cn. Tel: 0086-431-8516-8608. Fax: 0086-431-8516-8608.

Present Addresses

State Key Laboratory of Inorganic Synthesis and Preparative Chemistry, College of Chemistry, Jilin University, Changchun 130012, P. R. China

Author Contributions

The manuscript was written through contributions of all authors. All authors have given approval to the final version of the manuscript. ‡These authors contributed equally.

Notes

The authors declare no competing financial interests.

ACKNOWLEDGMENTS

We thank the State Basic Research Project of China (Grant No. 2014CB931802) and the National Natural Science Foundation of China (Grant No: 21320102001).

REFERENCES

- (1) (a) Zhu, Q.-L.; Xu, Q., *Energy Environ. Sci.*, **2015**, 8, 478-512; (b) Schlapbach, L.; Züttel, A., *Nature*, **2001**, 414, 353-358; (c) Edwards, P. P.; Kuznetsov, V. L.; David, W. I. F.; Brandon, N. P., *Energ. Policy*, **2008**, 36, 4356-4362; (d) Satyapal, S.; Petrovic, J.; Read, C.; Thomas, G.; Ordaz, G., *Catal. Today*, **2007**, 120, 246-256.
- (2) (a) Rosi, N. L.; Eckert, J.; Eddaoudi, M.; Vodak, D. T.; Kim, J.; O'Keeffe, M.; Yaghi, O. M., *Science*, **2003**, 300, 1127-1129; (b) Seayad, A. M.; Antonelli, D. M., *Adv. Mater.*, **2004**, 16, 765-777; (c) Suh, M. P.; Park, H. J.; Prasad, T. K.; Lim, D. W., *Chem. Rev.*, **2012**, 112, 782-835; (d) Graetz, J., *Chem. Soc. Rev.*, **2009**, 38, 73-82.
- (3) (a) Jiang, K.; Xu, K.; Zou, S.; Cai, W.-B., *J. Am. Chem. Soc.*, **2014**, 136, 4861-4864; (b) Boddien, A.; Junge, H., *Nat. Nanotechnol.*, **2011**, 6, 265-266; (c) Wang, Z. L.; Yan, J. M.; Ping, Y.; Wang, H. L.; Zheng, W. T.; Jiang, Q., *Angew. Chem. Int. Ed.*, **2013**, 52, 4406-4409; (d) Zhu, Q.-L.; Tsumori, N.; Xu, Q., *Chem. Sci.*, **2014**, 5, 195-199; (e) Grasmann, M.; Laurenczy, G., *Energy Environ. Sci.*, **2012**, 5, 8171-8181.
- (4) (a) Gu, X.; Lu, Z.-H.; Jiang, H.-L.; Akita, T.; Xu, Q., *J. Am. Chem. Soc.*, **2011**, 133, 11822-11825; (b) Enthaler, S.; von Langermann, J.; Schmidt, T., *Energy Environ. Sci.*, **2010**, 3, 1207-1217.
- (5) (a) Fellay, C.; Dyson, P. J.; Laurenczy, G., *Angew. Chem. Int. Ed.*, **2008**, 47, 3966-3968; (b) Johnson, T. C.; Morris, D. J.; Wills, M., *Chem. Soc. Rev.*, **2010**, 39, 81-88; (c) Fukuzumi, S.; Kobayashi, T.; Suenobu, T., *J. Am. Chem. Soc.*, **2010**, 132, 1496-1497; (d) Boddien, A.; Loges, B.; Gaertner, F.; Torborg, C.; Fumino, K.; Junge, H.; Ludwig, R.; Beller, M., *J. Am. Chem. Soc.*, **2010**, 132, 8924-8934.
- (6) Zhu, Q.-L.; Li, J.; Xu, Q., *J. Am. Chem. Soc.*, **2013**, 135, 10210-10213.
- (7) (a) Song, F.-Z.; Zhu, Q.-L.; Tsumori, N.; Xu, Q., *ACS Catal.*, **2015**, 5, 5141-5144; (b) Wang, Z.-L.; Wang, H.-L.; Yan, J.-M.; Ping, Y.; O, S.-I.; Li, S.-J.; Jiang, Q., *Chem. Commun.*, **2014**, 50, 2732-2734.
- (8) Dai, H.; Xia, B.; Wen, L.; Du, C.; Su, J.; Luo, W.; Cheng, G., *Appl. Catal. B*, **2015**, 165, 57-62.
- (9) (a) Tuel, A.; Farrusseng, D., *New J. Chem.*, **2016**, 40, 3933-3949; (b) Corma, A.; Garcia, H., *Chem. Soc. Rev.*, **2008**, 37, 2096-2126.
- (10) (a) Guczi, L.; Kiricsi, I., *Appl. Catal. A*, **1999**, 186, 375-394; (b) Li, X.; Iglesia, E., *Chem. Commun.*, **2008**, 594-596.
- (11) Guzman, J.; Gates, B. C., *Dalton. Trans.*, **2003**, 3303-3318.
- (12) Gallezot, P., in *Post-Synthesis Modification I*, Springer Berlin Heidelberg, **2002**, vol. 3, pp. 257-305.
- (13) (a) Choi, M.; Wu, Z.; Iglesia, E., *J. Am. Chem. Soc.*, **2010**, 132, 9129-9137; (b) Goel, S.; Wu, Z. J.; Zones, S. I.; Iglesia, E., *J. Am. Chem. Soc.*, **2012**, 134, 17688-17695; (c) Goel, S.; Zones, S. I.; Iglesia, E., *J. Am. Chem. Soc.*, **2014**, 136, 15280-15290; (d) Wu, Z.; Goel, S.; Choi, M.; Iglesia, E., *J. Catal.*, **2014**, 311, 458-468.
- (14) (a) Kim, J.; Jo, C.; Lee, S. and Ryoo, R., *J. Mater. Chem. A*, **2014**, 2, 11905-11912. (b) Ahn, J. H.; Kolvenbach, R.; Al-Khattaf, S. S.; Jentys, A. and Lercher, J. A., *ACS Catal.*, **2013**, 3, 817-825.
- (15) Keller, T. C.; Desai, K.; Mitchell, S.; Pérez-Ramírez, J., *ACS Catal.*, **2015**, 5, 5388-5396.
- (16) Yamada, Y. M. A.; Yuyama, Y.; Sato, T.; Fujikawa, S.; Uozumi, Y., *Angew. Chem.*, **2014**, 126, 131-135.
- (17) Loges, B.; Boddien, A.; Junge, H.; Beller, M., *Angew. Chem. Int. Ed.*, **2008**, 47, 3962-3965.
- (18) (a) Bi, Q. Y.; Du, X. L.; Liu, Y. M.; Cao, Y.; He, H. Y.; Fan, K. N., *J. Am. Chem. Soc.*, **2012**, 134, 8926-8933; (b) Ojeda, M.; Iglesia, E., *Angew. Chem. Int. Ed.*, **2009**, 48, 4800-4803; (c) Bulushev, D. A.; Jia, L.; Beloshapkin, S.; Ross, J. R. H., *Chem. Commun.*, **2012**, 48, 4184-4186.

Table of Contents

